Journal of Power Sources 194 (2009) 119–129

Contents lists available at ScienceDirect

Journal of Power Sources

journal homepage: www.elsevier.com/locate/jpowsour

Review

Review on microfabricated micro-solid oxide fuel cell membranes

Anna Evans*, Anja Bieberle-Hütter, Jennifer L.M. Rupp, Ludwig J. Gauckler

Nonmetallic Inorganic Materials, Department of Materials, ETH Zurich, Wolfgang-Pauli-Strasse 10, HCI G 536, CH–8093 Zurich, Switzerland

ARTICLE INFO

Article history:
Received 10 December 2008
Received in revised form 17 February 2009
Accepted 23 March 2009
Available online 2 April 2009

Keywords:
Micro-solid oxide fuel cell
MEMS
Microfabrication
Miniaturization
Thin film deposition

ABSTRACT

Micro-solid oxide fuel cells (μ-SOFC) are promising power sources for portable electronic devices. This review presents the current status of development of microfabricated micro-solid oxide fuel cell membranes for power delivery. The μ-SOFC membranes are developed using micro-electro-mechanical system (MEMS) fabrication and machining techniques. The different designs of free-standing μ-SOFC membranes and μ-SOFCs deposited on porous substrates are presented. The materials used in the μ-SOFC anode, electrolyte and cathode are discussed and compared along with their microstructures. The electrical performance data of the different μ-SOFC designs are compared and discussed. High μ-SOFC performances of 677 mW cm^{-2} were demonstrated at temperatures as low as 400 °C.

Contents

1. Introduction

The importance of small-scale energy-delivering devices has increased over the past few years with the growing demand for power sources in portable electronic devices. Miniaturized fuel cell systems promise to provide longer and more reliable power than batteries. Prototype micro-fuel cells exist for proton exchange membrane fuel cells (PEMFC) and direct methanol fuel cells (DMFC) which are conventionally used in portable applications due to their low-temperature operation (50–100 °C) [1]. Micro-solid oxide fuel cells (μ-SOFC) have potentially several advantages over other fuel cell systems and secondary battery technologies. SOFCs can operate on high-energy density hydrocarbon fuels such as propane and butane, whereas PEMFCs require pure hydrogen as a fuel gas. The latter involves not only expensive fuel reforming, but also critical transport and storage problems. The drawbacks of DMFCs are the need for concentrated toxic methanol to achieve beneficial energy densities and the problem of methanol cross-over [2]. Furthermore, both PEMFC and DMFC require expensive Pt catalysts for efficient operation. The potentials of the different fuel cell types become obvious when comparing the specific energies and the energy densities of these systems. Fig. 1 shows that μ-SOFC systems are predicted to have the highest specific energy and energy density, i.e. they are lighter and smaller, compared to DMFC and PEMFC systems. SOFCs are also predicted to achieve three to four times the energy density of lithium-ion or nickel-metal hydride batteries and are therefore considered an attractive alternative power supply source [3].

Conventional SOFCs are used for stationary applications with power ratings in the kilowatt to megawatt range and operate at temperatures from 800 to 1000 °C [4]. In contrast to these large systems, the operating temperature of micro-solid oxide fuel cells

* Corresponding author. Tel.: +41 44 632 3763; fax: +41 44 632 1132.
E-mail address: anna.evans@mat.ethz.ch (A. Evans).

0378-7753/$ – see front matter © 2009 Elsevier B.V. All rights reserved.
doi:10.1016/j.jpowsour.2009.03.048

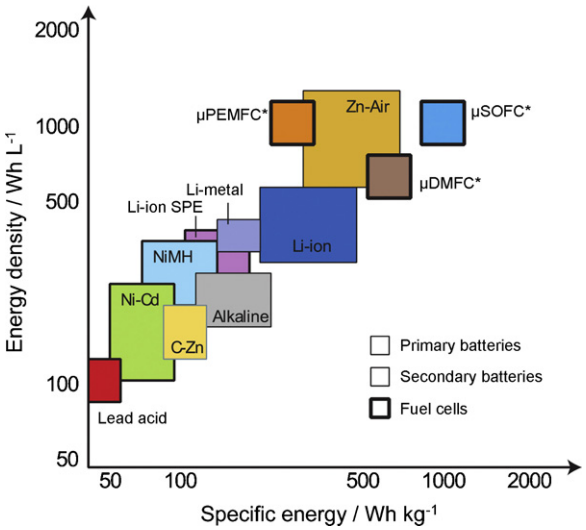

Fig. 1. Specific energy (per mass of device) and energy density (per volume of device) of several portable energy sources [44]. * Indicates estimated values, as these devices are not fully developed yet.

(μ-SOFCs) can be reduced to below 600 °C, and down as low as 350 °C. This can be achieved by reducing the electrolyte layer thickness, i.e. by decreasing the diffusion path length of the oxygen ions, and by optimizing of the materials and their properties. Micro-SOFC systems are therefore promising power sources for portable electronic devices with power requirements of between 1 and 20 W, such as mobile phones, personal digital assistants (PDAs), laptops, video camcorders and battery chargers, as well as small medical and industrial devices [5–7].

Such μ-SOFC systems have been proposed by Lilliputian Systems (Massachusetts, USA) [8,9] and by a Swiss university consortium under the lead of ETH Zurich [5,10–27]. The so-called ONEBAT μ-SOFC system from Switzerland consists of a μ-SOFC membrane, a gas-processing unit for fuel reforming and post-combustion, and a thermal system which includes insulation materials [5]. ONEBAT is the synthetic name of the system and is not an abbreviation.

While only two research groups worldwide are focusing on the development of an entire μ-SOFC system, many groups are currently studying μ-SOFC membranes for these systems [11,20,28–30]. Different designs of μ-SOFC membranes have been proposed in the literature; a brief overview of their fabrication methods is given by Jasinski [31]. In the dual gas-chamber μ-SOFC concept, the fuel and oxidant gases are separated by the electrolyte layer, which is a gas-tight seal. The driving force in such a μ-SOFC is the difference in the oxygen partial pressure between the anode (low pO_2) and the cathode (high pO_2). There are two possible designs for dual gas-chamber μ-SOFCs: planar and tubular. Planar μ-SOFCs consist of a layered structure of electrodes and electrolyte with a supporting substrate which can be microstructured [11,20,28–30]. Tubular μ-SOFCs consist of small, needle-like tubes bundled together into a stack. They have been studied by Sammes et al. [32] and Suzuki et al. [33,34]. In the tubular concept, the microtubular electrochemically active cells are obtained by extrusion and dip-coating processes of very small ceramic tubes (diameter < 0.4 mm). The tubular configuration is well suited to repeat cell cycling under rapid changes in the operating temperature, since the temperature gradient only prevails in the direction perpendicular to the tube. Problems related to heat stress (cracking), for example, can thus be overcome. These tubular μ-SOFC systems are not considered in this current review, however, as they do not include microfabrication in the classical sense but rely on conventional ceramic technology.

This review paper gives an overview of microfabricated dual gas-chamber μ-SOFC membranes with a planar geometry of the electrochemically active layers. The "micro" aspect should be emphasized, since this refers to two factors. On the one hand, the μ-SOFC membranes are developed on the basis of MEMS (micro-electro-mechanical system) microfabrication and machining techniques, such as thin film deposition and micropatterning. On the other hand, the size of the individual electrochemically active μ-SOFC system components, e.g. the active membrane thickness, is within the micrometer range, whereas the dimensions of the material microstructure (e.g. grain size and layer thickness) and patterned structures can extend down to the nanometer scale. The μ-SOFC membranes are discussed with regard to their design, the materials used in both the electrochemically active part and the substrate, and the electrochemical performances achieved.

2. Microfabricated μ-SOFC membranes

2.1. Membrane designs

The design of the planar μ-SOFC membrane comprises three active layers: two porous electrodes (anode and cathode) which are separated by a dense oxygen-ion conducting electrolyte. This trilayer structure is referred to as the positive electrode–electrolyte–negative electrode (PEN) element, and can either be part of a free-standing membrane, i.e. supported by a substrate material, or deposited directly onto a porous electrode support, as shown in Fig. 2.

The thermal and mechanical stability, chemical compatibility during preparation and operation, reliability and electrochemical performance of microfabricated μ-SOFC membranes are scale-dependent properties, and hence, the structural design of the electrochemically active membrane must be configured carefully. Srikar et al. [35] examined the influence of structural design in terms of thermal behavior, mechanical stability and reliability, e.g. the effect of electrolyte thickness on the electrochemical performance of electrolyte-supported μ-SOFCs. On the one hand, the electrolyte must be dense, so as to ensure a gas-tight layer and, on the other hand, a thin electrolyte is preferential, since the ohmic resistance scales with the electrolyte thickness. Fleig et al. [36] performed numerical calculations to analyze the influence of the electrolyte thickness on the resulting ohmic resistance. They concluded that electrolyte films with a thickness below the particle-to-particle distance of the electrode (300 nm) do not lead to a reduction in the ohmic resistance due to current constrictions at the triple phase boundaries. Hence, electrolyte thin films for μ-SOFC should not be as thin as possible, but ought to be thicker than ~300 nm.

The combination of thin film deposition and micro-machining techniques offers numerous possibilities for μ-SOFC processing. Sputtering, lithography and etching processes can be used to

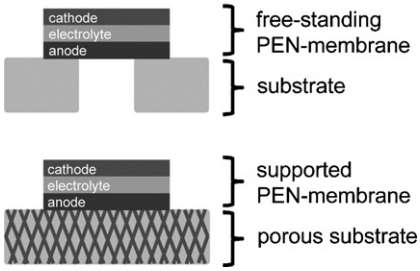

Fig. 2. Schematic drawing of a free-standing PEN-membrane (top) and a PEN-membrane on a porous substrate (bottom).

Table 1
Overview of different designs for micro-solid oxide fuel cells (μ-SOFC). The PEN-element includes cathode, electrolyte and anode.

Reference	Description of μ-SOFC	Substrate	Total PEN thickness (μm)	Membrane geometry and area (mm^2)		Temp. range (°C)
Stanford Univ., USA Shim et al. [29]	Free-standing μ-SOFC membranes	Silicon wafer	0.2	Square	0.0004–0.01	265–350
ETH Zurich, Switzerland Muecke et al. [11]	Free-standing μ-SOFC membranes	Foturan® glass-ceramic	~1	Circular	0.008–0.03	300–600
Stanford Univ., USA Huang et al. [28]	Free-standing ultrathin μ-SOFC	Silicon wafer	0.2–0.3	Square	0.003 or 0.06	200–450
K.I.S.T., Korea Kwon et al. [40]	Free-standing thin film μ-SOFC	Silicon wafer	~1	Square	0.25–1	500
Stanford Univ., USA Su et al. [41]	μ-SOFC with free-standing corrugated membrane	Silicon wafer	0.3	Square	0.36–4	400–450
Pohang Univ., Korea Joo and Choi [42]	Free-standing μ-SOFC	Nickel plate	~4	Circular	7.1	450
EPF Lausanne, Switzerland Rey-Mermet et al. [20,43]	Free-standing μ-SOFC supported by a nickel grid anode	Silicon wafer	~1	Circular	19.6	450
Stanford Univ., USA Kang et al. [45]	Thin film μ-SOFC	Porous nickel	~20	Nanoporous metal substrate with 20–200 nm pores		350–550

design free-standing membranes for μ-SOFCs [11,20,28,30,37,38]. An overview of microfabricated μ-SOFCs with free-standing membranes or on porous substrates is listed in Table 1. Photos and schematic drawings of these μ-SOFCs are presented in order of increasing membrane size in Fig. 3. The different fabrication designs in terms of substrate material, and also membrane geometry and size are described in the following section.

Shim et al. [29] reported on the fabrication of free-standing μ-SOFC membranes deposited onto a silicon wafer with a silicon nitride buffer layer. The active area ranged from 20 μm × 20 μm to 100 μm × 100 × μm, and the PEN-element was 220 nm thick.

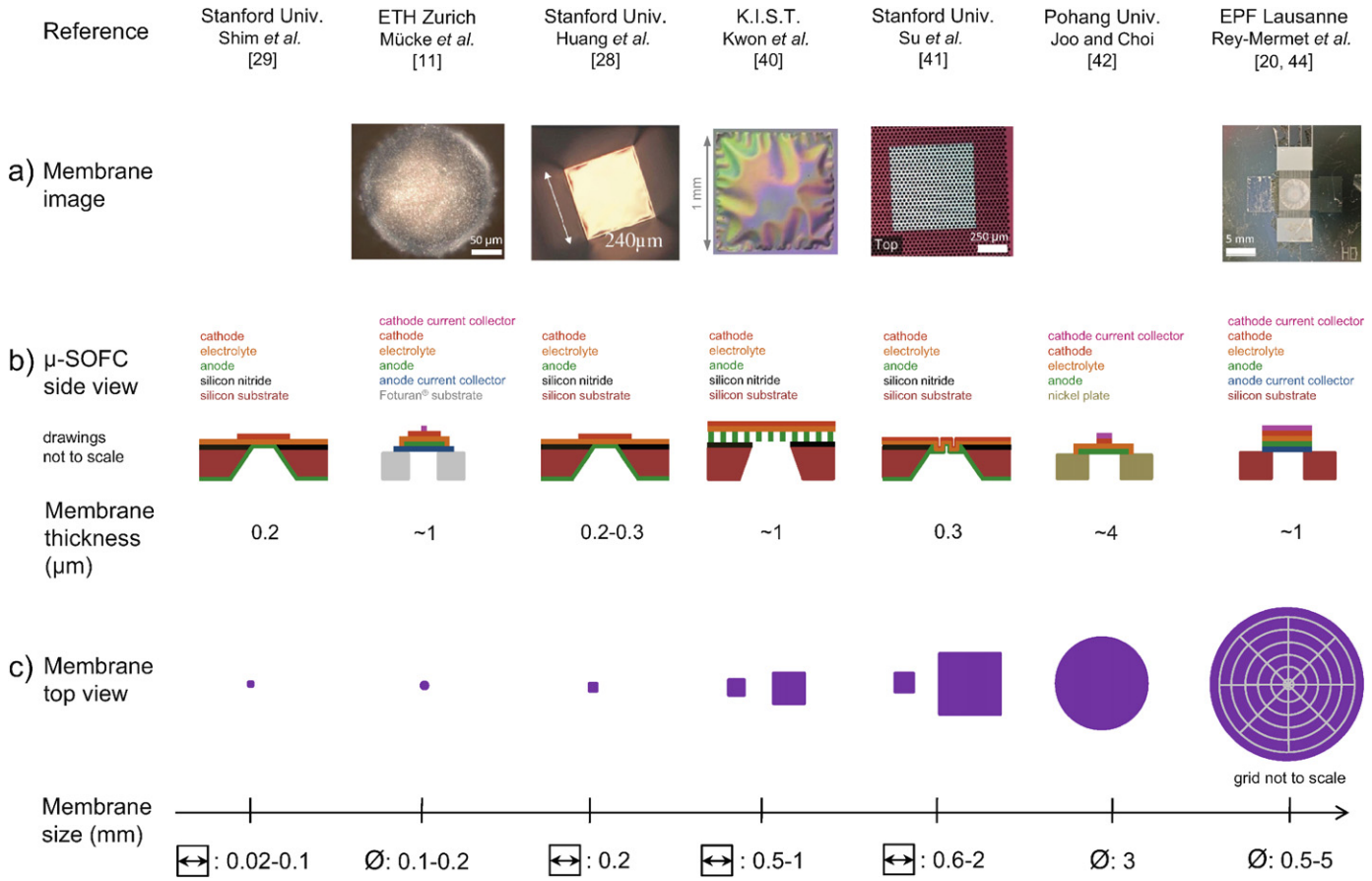

Fig. 3. Overview of different micro-solid oxide fuel cell free-standing membrane designs. (a) Images of the membranes. (b) Schematic drawing of the μ-SOFC components and design. (c) Schematic drawing of the shape and size of the free-standing membranes. Image by courtesy of Huang et al. [28], reproduced by permission of The Electrochemical Society. Image by Kwon et al. [40], reproduced by permission of the European Fuel Cell Forum. Image reprinted with permission from Su et al. [41], copyright 2008 American Chemical Society. Image by Rey-Mermet et al. [43], reproduced by permission of the Materials Research Society.

Table 2
Comparison of materials used as substrate, anode, electrolyte and cathode in μ-SOFCs.

Reference	Substrate	Anode	Electrolyte	Cathode
ETH Zurich [11]	Foturan® glass-ceramic	Pt	8YSZ	Pt, LSCF
Stanford Univ. [41]	Si wafer and Si_3N_4	Pt	8YSZ	Pt
Stanford Univ. [29]	Si wafer and Si_3N_4	Pt	8YSZ	Pt
Stanford Univ. [28]	Si wafer and Si_3N_4	Pt	8YSZ CGO	Pt
K.I.S.T. [40]	Si wafer and Si_3N_4	Ru	8YSZ	Pt
EPF Lausanne [20,43]	Si wafer and SiO_2	Pt	8YSZ	Pt
Pohang Univ. [42]	Nickel plate	Ni	CGO	Pt, LSCF
Stanford Univ. [45]	Porous Ni substrate acts as anode	Ni	8YSZ	Pt

8YSZ stands for 8 mol% Y_2O_3-stabilzed ZrO_2.

These μ-SOFCs were tested successfully between 265 and 350 °C.

The micro-solid oxide fuel cells developed at ETH Zurich [5,11] consist of anode, electrolyte and cathode thin films deposited on a Foturan® glass-ceramic substrate or passivated Si single crystals. The total thickness of the PEN thin films is approximately 1 μm. The circular free-standing membranes have a diameter of 100–200 μm. In the current design, three μ-SOFCs are arranged on a 1 cm × 1 cm Foturan® chip [11]. These μ-SOFCs have operating temperatures of between 300 and 600 °C. It is worth mentioning that these are the only μ-SOFCs that use the photostructurable Foturan® glass-ceramic as a substrate.

Huang et al. [28,39] from Stanford University fabricated ultrathin μ-SOFCs on a silicon substrate by microfabrication technology. The total thickness of the PEN-element does not exceed 300 nm. One 4-inch silicon wafer contains 832 active membranes with dimensions ranging from 50 μm × 50 μm to 240 μm × 240 μm. These fuel cells can operate at low temperatures of between 200 and 400 °C.

Kwon et al. [40] reported a different fabrication approach to thin film μ-SOFCs on a silicon substrate, whereby patterned anodized aluminum oxide is used as a template to obtain regular gas channels. Subsequently, the anode, electrolyte and cathode are deposited on the porous structure. The free-standing membrane area is either 500 μm × 500 μm or 1000 μm × 1000 μm. These μ-SOFCs can be operated at 500 °C without structural degradation.

A very recent publication by Su et al. [41] describes the fabrication of μ-SOFCs with a corrugated thin film membrane. This is achieved by patterning the silicon wafer with standard lithography and creating 10–40 μm deep trenches by reactive-ion etching. The electrolyte thin film is then deposited onto the silicon template. Etching with KOH and sputtering the electrodes leads to free-standing corrugated membranes with a total thickness of ~300 nm and a side dimension of up to 2 mm. These μ-SOFCs were operated successfully at 400–450 °C. The advantage of a corrugated membrane structure compared to a flat membrane design is that the electrochemically active area is larger than the projected area.

Recently, Joo and Choi [42] fabricated a μ-SOFC based on a nickel substrate. The electrolyte and cathode thin films are deposited on a porous nickel support which also acts as the anode. The active membrane area is ~7 mm^2, and the cells operate at 450 °C.

A completely different μ-SOFC fabrication approach is described by Rey-Mermet and Muralt [20,21,43,44]. These μ-SOFCs are based on a silicon wafer substrate and have free-standing membranes with a diameter of up to 5 mm. This is possible, since a nickel grid current collector with a hexagonal or spider web pattern with grid spacings in the 50–100 μm range serves to reinforce the membrane, i.e. to avoid buckling and cracking.

In 2006, Kang et al. [45] reported the fabrication of μ-SOFCs on a nanoporous nickel support structure which also acts as the anode. The gas channels within this nickel substrate have a diameter that gradually changes from 200 nm (on the gas delivery side) to 20 nm (on the electrolyte side). The larger nanoholes ought to enhance fuel delivery, whereas the 20 nm pores can be fully covered by a thin film electrolyte to ensure gas-tightness. These cells are operated in a temperature range of between 370 and 550 °C. Although these cells do not consist of a free-standing membrane, this approach should, however, also be considered for the fabrication of μ-SOFCs, since it provides the desired mechanical strength to support the thin film electrolyte.

To sum up, microfabricated μ-SOFC membranes as presented in the literature have thicknesses of 0.1–4 μm and are operated at temperatures of 200–550 °C. The overall design of the free-standing membranes as shown in Fig. 3 is realized with flat membrane layers. Only Su et al. [41] integrated a corrugated μ-SOFC membrane. According to Tang et al. [46] corrugated films are more reliable from a mechanical point of view, since the probability of failure (e.g. buckling and crack formation) is lower than in the flat thin films for the same thermal stress.

The main difference in the designs is the membrane size which varies from several hundred micrometers to a few millimeters. This wide range of sizes is due to two factors: firstly, thin films can easily suffer from pinholes. In the case of large membranes, a single pinhole can detrimentally affect the performance of the entire membrane. The probability of failure of this type is much lower for smaller areas and favors small membranes for μ-SOFC application. Secondly, however, the overall performance is directly related to the membrane area. Hence, many small membranes are required in order to obtain the same power output as for a large membrane. Small membranes thus have to be coupled and interconnected—and in this respect, larger membranes are favorable. This discussion shows that, in principle, large membranes would be best; however, membrane quality might limit the size. So far, no rules relating to ideal membrane size can be drawn up, since size limitations are strongly conditioned by the fabrication methods. Further and more detailed studies are required.

2.2. Materials and microstructures

The materials used for the anode, electrolyte and cathode of μ-SOFC membranes should have suitable electrical (electronic and/or ionic) conduction properties as well as adequate chemical compatibility with the components they are in contact with and structural stability at both fabrication and operation temperatures (<600 °C). Thin film materials have microstructural features which are in the nanometer range. At the operating temperatures, these materials should not undergo drastic changes in their microstructure and coarsening due to Ostwald ripening is one of the concerns. The materials and their properties should be stable at least for the expected lifetime of the device. An overview of the different materials used in the microfabricated μ-SOFC membranes and substrates is given in Table 2. The state-of-the-art electrolyte material is yttria-stabilized zirconia (YSZ). As electrode materials, most studies used precious metals, mainly Pt, due to its simplicity, good availability and good catalytic properties. Please note that only small amounts of material are required for μ-SOFC membranes, and costs are not of major concern here at the moment. For the

Table 3
Overview of deposition techniques used for deposition of anode, electrolyte and cathode thin films for μ-SOFC.

Reference	Deposition technique		
	Anode	Electrolyte	Cathode
ETH Zurich [11]	dc-sputtering	SP, PLD	SP, dc-sputtering
Stanford Univ. [28,29,41,45]	dc-sputtering	rf-sputtering, dc-sputtering, ALD	dc-sputtering
K.I.S.T. [40]	ALD	PLD	dc-magnetron-sputtering
Pohang Univ. [42]	Screen-printing	PLD	dc-sputtering
EPF Lausanne [20,43]	dc-magnetron-sputtering	rf-sputtering	dc-magnetron-sputtering

Abbreviations: ALD: atomic layer deposition, dc: direct current, rf: radio frequency, SP: spray pyrolysis, PLD: pulsed-laser deposition.

future, electrode materials other than precious metals will most probably be used due to cost issues and performance. Perovskites or cermets could be alternatives similar to the ones used in traditional SOFC designs; however, completely different groups of materials might also gain significance when the operating temperature is lowered. When it comes to the substrate material, many different materials have been suggested by the different groups, ranging from silicon and glass ceramics through to metals. So far there is no consensus on which is the best substrate material.

The thin film deposition techniques used by the different research groups are summarized in Table 3. Both vacuum deposition methods such as sputtering and pulsed-laser deposition (PLD), and non-vacuum deposition techniques, such as atomic layer deposition (ALD) and spray pyrolysis (SP), are frequently used. The choice of deposition method has an influence on the crystallinity and the microstructure of the thin film: non-vacuum methods usually result in amorphous thin films which can be transformed into crystalline films via annealing; vacuum methods usually lead to crystalline thin films forming during deposition already. The microstructures are mostly bricklayer-type for non-vacuum methods and columnar following the annealing of vacuum-deposited thin films. These types of microstructures are maintained under μ-SOFC operation. Details of the experimental setups and working principles of thin film preparation techniques (sputtering, spray pyrolysis and pulsed-laser deposition) can be found elsewhere [47,48].

In the following, we will discuss PEN-element and substrate materials. By comparison to a recent review on thin films for μ-SOFCs by Beckel et al. [13], the main focus here is on materials which are and can be used in actual μ-SOFC approaches as given in Table 1 and Fig. 2.

2.2.1. PEN-element materials

2.2.1.1. Anode. Anodes should be porous in order to allow a sufficient gas exchange at the gas–electrolyte–anode interface, i.e. they should have a large triple phase boundary length (TPB). The anode should also be catalytically active towards fuel oxidation. Furthermore, the material must be a good mixed electronic and ionic conductor. In addition, the anode material should not react chemically with the substrate or other membrane thin films that are in contact with it.

Sputtered platinum is the most frequently used anode material for investigating the cell performance of the μ-SOFCs reviewed here [11,20,28,29,41], since platinum displays good catalytic activity. This is an expensive noble metal, however, and the microstructures of nanoporous pure platinum electrodes can suffer from degradation due to Ostwald ripening as a function of temperature, time, and film thickness [49,50].

Fig. 4 shows an example of a platinum anode consisting of a porous network. The degree of porosity is a function of the thickness and the annealing temperature and annealing time of the platinum thin film [50]. This is important in two respects: on the one hand, numerous pores are required to guarantee sufficient fuel gas access and a large triple phase boundary length, whereas, on the other hand, a closed platinum-network is necessary for in-plane electronic conduction. Optimal parameters need to be established, since grain growth during μ-SOFC operation may lead to an increasing polarization resistance over time.

Wang et al. [49] investigated the thermal stabilities of nanoporous sputtered Pt–Ni alloys compared to pure Pt thin films. Grain growth in platinum thin films leads to reduced porosity and increased polarization resistance after annealing at 400–600 °C. The microstructure of the Pt–Ni thin films, however, remained unchanged (i.e. no coarsening), and these alloy cathodes showed an increased stability with operating time and higher μ-SOFC performances between 350 and 550 °C. Hence, alloy materials might be a good material class for μ-SOFC anodes.

The electrochemical properties of nickel pattern anodes with well-defined triple-phase boundary lengths were investigated by Mizusaki et al. [51] and Bieberle et al. [52] with the main focus on kinetic studies. For μ-SOFC membrane application, these electrodes have a too small triple phase boundary length and thus do not qualify as good anodes. Porous metallic nickel has been used as an anode in μ-SOFCs by Joo and Choi [42] and Kang et al. [45]. Metallic nickel has sufficient catalytic activity, but grain coarsening at elevated temperatures and a different thermal expansion coefficient from electrolyte materials are a concern when it comes to its use as an anode in μ-SOFCs. Therefore, preferential use is made of nickel, in combination with a ceramic material to form a porous ceramic–metal composite in which the rigid ceramic grain network prevents excessive nickel grain growth [53].

In Ni–YSZ cermets, the electronically conducting nickel forms a pathway for electrons, whereas the YSZ ceramic is ionically conducting. La O et al. [54] investigated the microstructure of radio frequency (rf)-sputtered Ni–YSZ cermets for μ-SOFC anodes. These porous Ni–YSZ films consisted of nano-sized columnar grains and showed no cracks after thermal treatment at 600 °C under a reducing atmosphere.

Muecke et al. [12] measured the electrochemical performance of nanocrystalline Ni–CGO anodes with a thickness of 500–800 nm prepared by spray pyrolysis (SP) and pulsed-laser deposition (PLD) on CGO pellets. The polarization resistance of sprayed Ni–CGO (60/40 vol.%) decreased from 1.73 to 0.34 Ω cm^2 with a grain

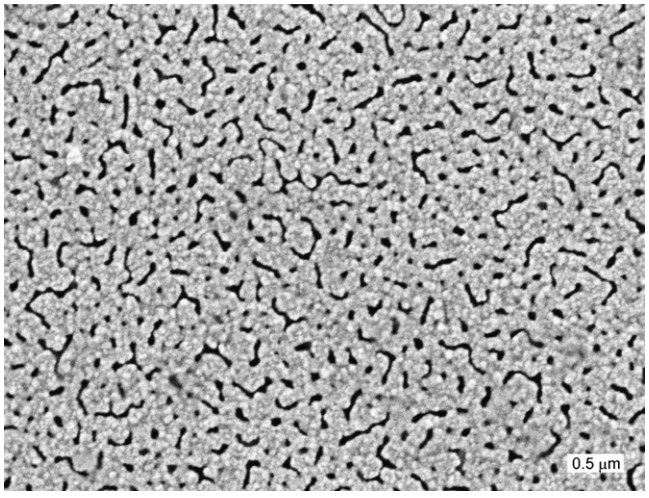

Fig. 4. SEM image of a platinum thin film sputtered on Foturan® annealed at 600 °C for 4 h [50]. The Pt-network covers 87.5% of the area. The dark areas are pores (image by courtesy of Galinski, ETH Zurich).

size decreasing from 53 to 16 nm respectively, at 600 °C. The thin films prepared by pulsed-laser deposition showed a columnar microstructure. The polarization resistance of the Ni–CGO (49/51 vol.%) anodes was 0.68 Ω cm^2 (at 600 °C) and thus comparable to the sprayed thin films [12]. Furthermore the electrochemical performance of the thin films was similar to state-of-the-art thick film anodes. These cermets have an increased interfacial contact area and are promising materials for applications in μ-SOFC anodes.

So far, only metallic thin films have been tested in complete μ-SOFC membranes (Table 2). However, several recent studies showed the potential of cermet anodes for μ-SOFC application. Hence, high-performance anodes can be expected to be integrated into μ-SOFC membranes in the near future. Electrochemical characterization of thin film anodes, for low temperature operation in particular, is very much in its initial stages. Specific anode materials for low operating temperature (i.e. <400 °C) have not yet been investigated.

2.2.1.2. Electrolyte. The electrolyte should be an ionic conductor with a dense microstructure in order to form a gas-tight layer to separate the oxidizing and reducing gas chambers. Electrolyte materials should be chemically stable in both oxidizing and reducing environments [55].

Yttria-stabilized zirconia (YSZ) [11,20,28,29,41,45] and cerium gadolinium oxide (CGO) [28,42] are the two electrolyte materials currently used in μ-SOFC membranes (Table 2). YSZ is a pure ionic conductor under the operating conditions of interest, whereas CGO solid solutions become mixed ionic-electronic conductors (MIEC), especially at the reducing anode side [14]. In thin film MIEC electrolytes, electronic leakage can occur [56]. This can be prevented by combining totally ionic conducting YSZ with mixed ionic-electronic conducting CGO to form bilayer electrolytes. Such ceria and yttria-based single and bilayer electrolyte thin films for low to intermediate temperature SOFCs were reported for example by Kleinlogel et al. [57,58] deposited on a porous LSCF cathode support and by Perednis et al. [59–62] deposited on a NiO–YSZ anode support.

In the following sections, the mechanical and thermal stabilities of free-standing CGO and YSZ thin film membranes are presented, and the influence of the microstructure on the electrical properties is discussed for both electrolyte materials.

Baertsch et al. [30] reported the fabrication and structural characterization of self-supporting CGO and YSZ electrolyte membranes for μ-SOFCs. The electrolyte thin film is deposited on a silicon nitride processed silicon substrate to form free-standing membranes with a thickness of between 0.1 and 1 μm. Investigations into the mechanical and thermal properties were performed for electrolyte membranes of sizes ranging from 65 μm × 65 μm to 1025 μm × 1025 μm. The stress measurements showed that the mechanical and thermal stabilities depend on the ratio of film thickness to free-standing membrane area. Considering the thermal expansion mismatch between YSZ and Si, it was surprising that large free-standing membranes could be fabricated and were able to withstand the elevated temperatures. Greenberg et al. [63] investigated the elasticity of a free-standing CGO electrolyte with thicknesses of between 400 and 800 nm deposited onto a silicon substrate. The rectangular membranes (260 μm × 300 μm) showed a reversible change in dimensions upon externally applied thermal stress. Quinn et al. [64] analyzed the residual stress and microstructure of 5 nm to 1 μm thick YSZ electrolytes sputter-deposited onto a silicon wafer. It was found that the residual stress could be tailored; since it is a function of the film thickness, sputter deposition parameters and post-annealing conditions.

There are many publications that discuss the influence of processing (i.e. deposition parameters), such as the doping content and annealing temperatures on the CGO and YSZ electrolyte microstructures and, hence, also on their electrical conductivity properties. An overview of the conductivity data for CGO thin films is given in [13], whereas the large scatter of conductivities for YSZ electrolytes has not yet been summarized.

The largest discrepancy in the microstructure is governed by the type of film formation – by a vacuum or a non-vacuum method – which normally gives rise to a crystalline or amorphous thin film, respectively. Residual amorphous phases may act as a third phase, alongside the grain and the grain boundary, having an impact on the electrical properties of electrolyte thin films. The post-annealing of thin films deposited by non-vacuum techniques is of the utmost importance for the future electric operation of the electrolyte. The occurrence of amorphous phases in addition to crystalline grain and grain boundary areas was proven for spray pyrolysis CGO-films by transmission electron microscopy [65]. The amorphous phases that remain within these electrolyte films affect the CGO grain growth kinetics, making for self-limited grain growth in parallel to crystallization [66,67]. Huang et al. [68] reported a 3–4 orders of magnitude higher ionic conductivity for CGO-films with <50 nm thickness by comparison to bulk CGO. This effect was attributed to the reduction in the cross-grain boundary resistances within the ultrathin films. Suzuki et al. [69] investigated the influence of the microstructure and electrical properties of nanocrystalline CGO electrolytes with a thickness of 100–600 nm spin-coated onto a sapphire substrate. The CGO grain growth kinetics is a function of the dopant concentration and the annealing temperature. An increase in ionic conductivity and a decrease in activation energy are observed for a decreasing grain size. Similar observations were reported by Rupp et al. [70] for dense nanocrystalline $Gd_{0.2}Ce_{0.8}O_{1.9-\delta}$ microstructures prepared by SP and PLD (with a thickness of 300–400 nm) in which the ionic conductivity is controlled by the grain boundaries. Investigations of the electrolytic domain boundary for these microstructures revealed a clear shift to a higher oxygen partial pressure with a decreasing grain size [14]. This indicates a change in the electrical conduction mechanisms of these mixed ionic-electronic conducting films.

All the above-mentioned thin film studies on CGO characterized the conductivity by a four-point dc method. Grain and grain boundary contributions could not be isolated. This drawback was overcome by Bieberle-Hutter et al. [71] who characterized sputtered CGO thin films by ac impedance using interdigitated Pt electrodes. Five impedance contributions were found and attributed to wiring, grain, grain boundary, current constriction, and the electrolyte/electrode interface. Also in this study higher conductivities were found than usually reported for CGO.

In 2000, Kosacki et al. [72] found that the conductivity of dense nanocrystalline YSZ prepared by spin coating is one order of magnitude higher than for microcrystalline YSZ, and concluded that electrical transport in nanocrystalline materials is dominated by grain boundary effects. In more recent publications by Joo and Choi [73], Heiroth et al. [74] and Infortuna et al. [10] for YSZ prepared by PLD, no such pronounced increase in the conductivity behavior was observed. Joo and Choi [73] reported that the ionic conductivity and the activation energy of the 600 nm YSZ thin films grown on sapphire substrates are nearly equal to those of bulk YSZ. Similar results were obtained by Heiroth et al. [74] who investigated amorphous and crystalline 8YSZ thin films (60–450 nm thickness) on sapphire single crystals: no significant enhancement of ionic conductivity due to the nanocrystalline microstructure was measured. Infortuna et al. [10] highlighted the importance of PLD processing parameters for obtaining YSZ with a dense microstructure and electrical conductivity suitable for thin film-based μ-SOFC.

Another possible origin of the increased electrical conductivity on the nanometer scale may be the strain inside the grains. Kosacki et al. [75] reported enhanced electrical conductivity of highly textured YSZ with thicknesses <60 nm. These thin films were void of "blocking" grain boundaries (i.e. grain boundaries perpendicular to

the current flow) and there was only a single interface between the YSZ electrolyte and the MgO substrate. It was therefore possible to attribute a significant contribution of the "nanoscale" effect to the interface conductivity. Very recently, Garcia-Barriocanal et al. [76] reported an extremely high lateral ionic conductivity for YSZ/strontium titanate (STO) epitaxial heterostructures. The combination of epitaxial strain and interfaces in YSZ/STO led to an ionic conductivity that was eight orders of magnitude higher than for YSZ. This remarkable increase may, however, include electronic conductivity in addition to ionic conduction.

The examples given above for YSZ and CGO show the importance of understanding the relationships between the electrolyte's microstructure such as its degree of crystallinity, grain size, strain within grains, dopant segregation and space charge, and its electrical properties. All the studies show that thin film microstructures are very different from bulk material with respect to grain size, degree of crystallinity, grain boundaries, etc. As a result, the properties of thin films are rather different from those of bulk material; for example, several references state a higher conductivity for thin films as compared to bulk material [68–72,75,76]. The reason for the higher conductivities could be strain, the degree of crystallinity, space charge or, grain size; no common explanation is so far to be found in the literature.

Proton-conducting electrolytes could be an alternative to YSZ and CGO. SOFCs with proton-conducting electrolytes potentially have lower operating temperatures, which results in reduced SOFC costs and easier thermal system management. A review on proton-conducting oxides was given by Kreuer [77]. Yttria-doped $BaZrO_3$-based electrolytes combine a high thermodynamic stability with a high proton conductivity of $0.01\,S\,cm^{-1}$ at 600 °C, and are therefore potential proton-conducting SOFC electrolyte materials [77]. Ranran et al. [78] investigated the electrochemical properties of proton-conducting 50 μm samarium-doped $BaCeO_3$ electrolyte films. The measured conductivity of $BaCe_{0.8}Sm_{0.2}O_{2.9}$ was $4.16 \times 10^{-3}\,S\,cm^{-1}$ at 500 °C. Zhu [79] developed two-phase ceramic composites with hybrid proton and oxygen-ion conduction properties. The combination of an ion-doped ceria and a proton-conducting Li-salt led to an ionic conductivity of $0.01\,S\,cm^{-1}$ at 400 °C [79]. The proton conduction may promote the electrode reactions and kinetics at the electrode–electrolyte interfaces due to the faster reactivity of small protons. This can result in higher SOFC current outputs.

2.2.1.3. Cathode. The cathode must be porous in order to ensure oxygen transport to the interface of the electrode and the electrolyte (i.e. a large triple phase boundary length). Cathode materials must be catalytically active towards oxygen reduction, and should show good mixed ionic-electronic conduction properties. Most of the microfabricated μ-SOFCs presented so far in the literature have used Pt as a cathode material [11,20,28,29,41,45]. Other common cathode materials in μ-SOFCs with operating temperatures of below 600 °C are ABO_3 perovskites such as lanthanum strontium cobalt oxide (LSC), lanthanum strontium cobalt iron oxide (LSCF) and barium strontium cobalt iron oxide (BSCF). Discussions of cathode reaction mechanisms (e.g. oxygen reduction pathways), and investigations of bulk diffusion and triple phase boundary lengths are beyond the scope of this review paper. For detailed electrochemical analyses using microelectrodes and patterned electrodes both with well-defined geometries, the reader is referred to [80–83]. The next section provides an overview of the electrochemical investigations carried out for μ-SOFC cathode materials.

Platinum electrodes for μ-SOFC have already been described in the anode Section 2.2.1.1. Hertz and Tuller [84] investigated nanocomposite Pt–YSZ thin film electrodes for μ-SOFC deposited on single crystal YSZ. The area-specific polarization resistances of Pt–YSZ microelectrodes (with well-defined geometries) were lower than $500\,\Omega\,cm^2$ at 400 °C. A major advantage of these Pt–YSZ nanocomposites compared to other cathode materials is that they can be used on the anode and the cathode side, since the two constituents are stable in both oxidizing and reducing atmospheres. In addition, these Pt–YSZ cermets show a reduced chemical degradation due to grain coarsening at temperatures below 600 °C.

Lanthanum strontium cobalt oxide (LSC) is a good mixed ionic-electronic conductor and displays good catalytic activity towards oxygen reduction. As shown by Bieberle-Hutter et al. [82,83], it is possible to prepare well-defined LSC patterned electrodes by photolithographic methods. This might be particularly important for use in μ-SOFCs where defined sizes of cathode material have to be applied. Peters et al. [85] reported very low polarization resistances for nanoporous $(La_{0.5}Sr_{0.5})CoO_{3-\delta}$ cathodes prepared by metallorganic deposition. The LSC films with thicknesses of between 200 and 300 nm deposited on YSZ and CGO had polarization resistances of as low as 146 and $130\,m\Omega\,cm^2$, respectively at 600 °C.

The oxygen exchange properties of mixed-conducting $La_{0.6}Sr_{0.4}Co_{0.2}Fe_{0.8}O_{3-\delta}$ (LSCF) on CGO electrolytes have been reported by Steele and Bae [86]. It was shown that the introduction of a dense LSCF layer between the CGO electrolyte and the porous LSCF cathode increased the interfacial contact area and led to resistivities that were two to three times lower. Prestat et al. [87,88] investigated the oxygen reduction at dense $La_{0.52}Sr_{0.48}Co_{0.18}Fe_{0.82}O_{3-\delta}$ cathodes with well-defined dimensions by means of Faradaic impedance simulations and experimental measurements. The LSCF films with thicknesses varying between 10 and 800 nm were pulsed-laser deposited onto CGO pellets. It was shown that the contribution of the surface pathway to the reaction was negligible due to the small triple phase boundary length and that the diffusion of oxygen essentially proceeds in the bulk LSCF. Similar results were reported by Baumann et al. [89] who investigated the oxygen reduction kinetics on geometrically well-defined dense thin film LSCF microelectrodes prepared by PLD on YSZ single crystals. Beckel et al. [90] investigated the microstructure and electrochemical performance of $La_{0.6}Sr_{0.4}Co_{0.2}Fe_{0.8}O_3$ cathode thin films prepared by spray pyrolysis on $Ce_{0.8}Gd_{0.2}O_{1.9}$ pellets. The annealing of LSCF had a strong influence on the microstructure and hence on the cathode performance too. Annealing at 650 °C led to the formation of smaller grains (~65 nm) and a finer microstructure compared to the LSCF samples annealed at 800 °C (grain size of ~124 nm). Therefore, the resulting area-specific resistance (ASR) is twice as high for the LSCF samples annealed at 800 °C due to the reduced triple phase boundary at the CGO electrolyte interface. Beckel et al. [90] also reported that the thin film deposition technique has an influence on cathode performance. LSCF thin films prepared by pulsed-laser deposition showed an ASR four times higher than those prepared by spray pyrolysis. This can be explained by the reduced in-plane conductivity of the PLD samples with a columnar microstructure. Another possible approach for increasing the electrochemical performance could be to introduce an additional layer between the cathode and the electrolyte. Beckel et al. [90] reported that a dense LSCF/CGO composite interlayer led to better oxygen transport properties at lower temperatures. Perry Murray et al. [91] used 20 μm thick LSCF and LSCF/CGO cathodes deposited onto a YSZ electrolyte to investigate zirconate formation at the interface. The interaction of LSCF with YSZ led to a reduced performance due to resistive zirconate poisoning under the μ-SOFC operating conditions. Similar chemical behavior can be expected for LSCF and YSZ thin films. This problem could be solved by the use of LSCF/CGO composite cathodes or the addition of a CGO interlayer to act as a diffusion barrier.

The mixed-conducting $Ba_{0.5}Sr_{0.5}Co_{0.8}Fe_{0.2}O_{3-\delta}$ (BSCF) has also been investigated as a potential cathode material. Shao and Haile [92] reported low polarization resistances of $0.51\,\Omega\,cm^2$

at 500 °C for porous 10 μm thick BSCF cathodes deposited on samaria-doped ceria electrolyte. The excellent performance of BSCF is attributed to the high oxygen diffusion rate through the material. Baumann et al. [93,94] reported an extremely low surface exchange resistance of 0.09 Ω cm^2 at 750 °C for 100 nm thick $Ba_{0.5}Sr_{0.5}Co_{0.8}Fe_{0.2}O_{3-\delta}$ microelectrodes, indicating a catalytic activity 50 times greater than for LSCF with respect to oxygen reduction reactions.

The examples given above show that Pt has been widely used as μ-SOFC cathode, but that other thin film materials have also been studied intensively. This is important, since the cathode is generally considered as the limiting factor in μ-SOFC performance [15]. The literature shows that, in the same way as for the electrolyte, the microstructure (grain size and shape) has a considerable effect on the properties of the cathode material. Chemical interaction of the cathode material with the adjacent electrolyte material is of great importance, especially until the operating temperature can be considerably lowered. Up till now, no studies exist in which cathode materials have been investigated specifically for the extremely low temperatures, i.e. below 500 °C, which are of interest for μ-SOFC application.

2.2.2. Substrate materials

The materials used as substrates in μ-SOFCs should be inert in order to avoid poisoning the thin electrochemically active films deposited on them, and they should be thermally and mechanically stable within the μ-SOFC manufacturing and operating temperature ranges [55]. One very important criterion is that they must be able to be structured by microfabrication techniques, i.e. it must be possible to etch holes in the substrate in order to free the electrochemically active cell components for the gas supply to both sides of the fuel cell membrane. The μ-SOFCs presented in this review are fabricated on the basis of three different substrate materials: Foturan® glass-ceramic, silicon wafers and metallic nickel. The implications of using these support structures are discussed in the following section.

The Foturan® substrate used in the μ-SOFCs developed by ETH Zurich [11] is a photostructurable glass-ceramic with a thermal expansion coefficient (8.6×10^{-6} K^{-1}) [37] close to that of the ceramic thin film materials. The micropatterning of Foturan® is achieved by exposing certain areas to UV-light, while the rest of the sample is covered by a mask. Subsequent annealing at 500 and 600 °C induces nuclei formation and crystallization, respectively, in the UV-exposed areas. These crystalline parts can be wet-etched with hydrofluoric acid 20 times faster than the unexposed glassy areas, in order to form gas channels and free-standing membranes. The use of hydrofluoric acid is, however, critical as it may attack the deposited thin films too. Since Foturan® is itself an electrical insulator, the fuel cell layers can be deposited directly onto the substrate and no additional insulating coating needs to be applied. Foturan® can be used for temperatures up to 600 °C. Higher temperatures lead to a softening and warpage of the glass-ceramic, which can cause cracks in the membranes.

Silicon wafers are also used as substrates for microfabricated μ-SOFC membranes [20,28,40,41]. The structuring of silicon single crystals is standard in the semi-conductor industry and hence the silicon etching techniques are well developed [95]. However, silicon structuring for high temperature applications and processes is more difficult. In order to use the semi-conducting silicon as a substrate, it must be covered by an electrical insulation layer, e.g. silicon nitride (Si_3N_4) or silicon dioxide (SiO_2), prior to deposition of the thin films in order to prevent short-circuiting. The low-stress silicon nitride also serves as a barrier to avoid any chemical reactions between the silicon substrate and the PEN materials. A detailed description of the silicon processing steps, including photolithographic patterning and etching, is given by Huang et al. [28] and Baertsch et al. [30]. A drawback of silicon is its low thermal expansion coefficient (2.6×10^{-6} K^{-1}) [96] compared to the thin films of the μ-SOFC membrane ($\sim$10–20 $\times 10^{-6}$ K^{-1}). Furthermore, the presence of pinholes within the insulation layer can cause an electrical breakdown between the μ-SOFC membrane and the silicon substrate. Hence, silicon can only be used as substrate if a good, pinhole-free insulation layer can be applied.

Finally, nickel was used as a substrate for μ-SOFC membranes. Recently, Joo and Choi [42] fabricated a porous nickel substrate from NiO by screen-printing and subsequent reduction under hydrogen. The resulting nickel film, which also acts as anode, is supported by a nickel plate. Kang et al. [45] developed a porous nickel substrate with a multistage nanohole array in which the diameter of the pores decreases from 200 to 20 nm over the thickness of the support. This was achieved by using a porous anodic aluminum oxide (AAO) mother structure, which was filled with poly(methylmethacrylate). The AAO template was removed under basic conditions, and the nickel is electroplated to give the nanoporous support. This μ-SOFC substrate fabrication does not include any complex lithography and etching steps, but the replication process is rather complicated.

So far, silicon wafers are the most widely used substrates in μ-SOFCs. The silicon wafers, Foturan® glass ceramic and nickel substrates all have advantages and disadvantages as mentioned before. No final decision can be made on the best choice of substrate material, since this also depends on the μ-SOFC stack design and consecutive issues such as bonding.

2.3. Electrical performance of μ-SOFC membranes

The driving force behind oxygen diffusion through the electrolyte is the oxygen partial pressure differential between the anode (low pO_2) and the cathode (high pO_2). The open-circuit voltage (OCV) corresponds to the potential across the μ-SOFC without any applied current. The electrical performance of a μ-SOFC is defined as the product of current density and voltage (i.e. OCV minus polarization losses). The OCVs and maximum power densities of different microfabricated μ-SOFCs are presented in Table 4. The electrochemical characteristics of the various μ-SOFCs are described in the following section.

Muecke et al. [11] fabricated a μ-SOFC consisting of a 550 nm thick 8YSZ electrolyte (prepared by PLD) and sputtered Pt electrodes deposited on a Foturan® glass-ceramic substrate. An OCV of 0.8 V and a peak performance of 4.9 mW cm^{-2} were reported at 500 °C. The electrolyte resistance of 0.054 Ω cm^2 (550 °C) is negligible compared to the electrode polarization of 19 Ω cm^2 (550 °C). The cathode reactions, in particular, limit the overall cell performance. An improvement was achieved by using an LSCF cathode deposited by spray pyrolysis (250 nm thickness), whereby a maximum power density of 10.1 mW cm^{-2} at 500 °C was obtained. The reduced OCV compared to the theoretical value was caused by pinholes present in the columnar YSZ electrolyte. By using sputtered Pt electrodes and a bilayer electrolyte of PLD–YSZ and SP–YSZ, an OCV of 1.06 V was obtained and the maximum power density reached 152 mW cm^{-2} at 550 °C.

Huang et al. [28] published very high power densities of 200 mW cm^{-2} (350 °C) and 400 mW cm^{-2} (400 °C) for μ-SOFCs developed by MEMS fabrication technologies. The μ-SOFC based on a silicon/silicon nitride substrate consisted of an ultrathin 8YSZ nanocrystalline electrolyte (50 nm thickness, rf-sputtering), a CGO interlayer (50 nm, dc-sputtering) and porous Pt electrodes (80 nm, dc-sputtering). A theoretical OCV of 1.1 V was obtained. In the absence of the CGO interlayer, the peak performance only reached 130 mW cm^{-2} at 350 °C. This can be explained by lower charge-transfer reaction rates at the interfaces between the nanocrystalline 8YSZ electrolyte and the nanoporous Pt cathode.

Table 4
Comparison of the open-circuit voltage and electrochemical performance of different μ-SOFCs.

Group	Ref.	μ-SOFC materials (anode–electrolyte–cathode)	Total electrolyte thickness (μm)	OCV (V)	Performance ($mW\,cm^{-2}$)	T (°C)	Testing conditions
ETH Zurich	Muecke et al. [11]	Pt–8YSZ–Pt	0.55	0.77	26.4	500	Cathode: air; anode: N_2:H_2 4:1
		Pt–8YSZ–LSCF	0.55	0.55	10.1	500	and 3 vol.% H_2O
		Pt–8YSZ/8YSZ–Pt	0.75	1.05	152.0	550	
	Huang et al. [28]	Pt–8YSZ–Pt	0.05	1.10	130	350	Cathode: air anode:
		Pt–8YSZ/CGO–Pt	0.1	1.10	200	350	pure H_2 and 3 vol.% H_2O
					400	400	
Stanford Univ.	Shim et al. [29]	Pt–8YSZ–Pt	0.22	1.10	270	350	Cathode: air; anode: pure H_2
	Su et al. [41]	Pt–8YSZ–Pt	0.07	1.09	677	400	Cathode: air; anode: pure H_2
					861	450	
	Kang et al. [45]	Ni–8YSZ–Pt	0.2	0.87	7	400	Cathode: air; anode: 97% N_2, 3% H_2
K.I.S.T.	Kwon et al. [40]	Ru–8YSZ–Pt	0.3	–	–	–	–
Pohang Univ.	Joo and Choi [42]	Pt–CGO–Pt	3	0.64	26	450	Cathode: air; anode: pure H_2 and 3 vol.% H_2O
EPF Lausanne	Rey-Mermet et al. [20]	Pt–8YSZ–Pt	0.75	0.28	–	450	Cathode: pure O_2; anode: Ar:H_2 4:1
	Rey-Mermet et al. [44]	Pt–8YSZ/8YSZ–Pt	0.5	0.85	0.02	500	Cathode: pure O_2; anode: pure Ar

Shim et al. [29] evaluated the performance of free-standing 8YSZ thin films prepared by ALD. The ultrathin (60 nm) YSZ electrolytes were sandwiched between two porous 80 nm Pt electrodes on a silicon substrate with a Si_3N_4 buffer layer. An OCV of 1.10 V and a power density of $270\,mW\,cm^{-2}$ were obtained at 350 °C. This high performance is presumably due to the low electrolyte resistance and fast electrode kinetics.

Recently, Su et al. [41] compared the performance of a corrugated YSZ membrane with porous Pt electrodes to a μ-SOFC with equivalent flat thin films. The electrochemically active area of the corrugated membrane is approximately five times larger than that for the planar geometry, and thus higher performances were achieved. Maximum power densities of the corrugated μ-SOFCs were $677\,mW\,cm^{-2}$ (400 °C) and $861\,mW\,cm^{-2}$ (450 °C), whereby the area in the unit refers to the projected area occupied by the free-standing membrane. Even higher performances could be achieved if the Pt deposited on the corrugated YSZ electrolyte has an improved conformal coverage.

Kang et al. [45] reported a maximum power density of $7\,mW\,cm^{-2}$ at 400 °C for a μ-SOFC with a 20 μm thick nanoporous nickel substrate. A 200 nm thick 8YSZ electrolyte and a porous Pt cathode were sputtered on top of this. An OCV of 0.87 V was obtained at 550 °C. This non-theoretical OCV may be caused by electrical pinholes in the 8YSZ electrolyte or by the low hydrogen partial pressure used for cell testing. The major drawback to this type of μ-SOFC is the low triple phase boundary density within the nanoporous nickel substrate which limits cell performance.

The μ-SOFCs developed by Kwon et al. [40] consisted of a silicon/silicon nitride substrate. A 15 nm thick ruthenium anode was deposited by atomic layer deposition onto the anodized aluminum oxide patterns. A dense 300 nm thick 8YSZ electrolyte (PLD) and a porous Pt cathode (100 nm thick, dc-magnetron sputtering) are deposited to form a free-standing μ-SOFC membrane. The electrochemical performance data of these μ-SOFCs have not been published yet.

Joo and Choi [42] reported an OCV of 0.64 V and a maximum power density of $26\,mW\,cm^{-2}$ at 450 °C for a μ-SOFC based on a nickel plate substrate (25 μm thick). The anode consisted of a porous nickel film prepared by screen-printing and subsequent reduction under hydrogen. The CGO electrolyte (3 μm thick) was deposited by pulsed-laser deposition and porous LSC was used as cathode. The low OCV may be attributed to structural defects within the CGO electrolyte.

Rey-Mermet and Muralt [20] published an OCV of 0.28 V at 450 °C for a 5 mm wide circular μ-SOFC membrane supported by a nickel grid. This nickel grid current collector, with either a hexagonal or spider web pattern, is electroplated onto a Si/SiO_2 substrate. The 750 nm thick 8YSZ electrolyte is deposited by rf-sputtering between the porous 100 nm Pt electrodes to form the free-standing membrane. The nickel grid increases the mechanical stability of the membrane, the OCV, however, is rather low due to pinholes and microcracks present within the electrolyte. An OCV of 0.85 V was achieved for similar μ-SOFCs with a smaller membrane (0.5 mm diameter) supported by a spider web nickel grid and consisting of a bilayer YSZ electrolyte [44]. The performance only attained $19\,\mu W\,cm^{-2}$ at 500 °C due to the high internal resistance of the cathode current collector.

A direct comparison of the different μ-SOFC membranes presented in this section with respect to performance is not possible on account of the different conditions (i.e. temperature, oxidant and fuel gas) employed for cell testing. It is however possible to summarize the main factors in favor of a high μ-SOFC membrane performance: the electrolyte has to be completely gas-tight, crack-free and as thin as possible. Gas leakage through pinholes and cracks causes a reduction in the open-circuit voltage. A good

means of minimizing this problem is the use of multilayer thin film electrolytes as shown by Muecke et al. [11] and Huang et al. [28]. The incorporation of CGO in addition to YSZ electrolyte also resulted in a higher performance due to a better charge transfer on the cathode side of the fuel cell [28]. It is well known that the performance of the μ-SOFCs is limited especially by the high cathode resistance. The incorporation of cathode materials with a lower polarization is required in future. In addition, it was shown that an increase in the active membrane area through the use of corrugated electrolytes is the most efficient means of obtaining a high performance: Su et al. [41] measured a sensationally high power output of 677 mW cm^{-2} at 400 °C. The high performances of individual microfabricated membranes at low SOFC temperatures (350–550 °C) indicate that the use of μ-SOFC stacks would provide a sufficient power supply for portable devices.

No durability tests on the individual components and on an integrated μ-SOFC system have been reported yet. The performance of these μ-SOFC components under longer operating conditions is not known, nor is their behavior during and after cyclic operation, especially after complete shut downs and restarts.

3. Conclusion

Today, μ-SOFC membranes are fabricated using a combination of thin film deposition and MEMS technologies. The free-standing electrochemically operated μ-SOFC membranes with diameters ranging from 20 μm to 5 mm are mechanically much more stable than would be expected from the stresses that have to be accommodated due to the thermal expansion mismatch between the materials.

A good μ-SOFC membrane should have a large active area. This can be achieved with free-standing corrugated membranes. Furthermore a thin, but gas-tight electrolyte is required in order to minimize the ohmic losses. The deposition of multilayer electrolytes – even consisting of several materials (YSZ and CGO) – is a possible means of preventing pinholes. The electrodes should have a large triple phase boundary length, and the materials must be catalytically active towards fuel oxidation (anode) and oxygen reduction (cathode), and display good mixed ionic-electronic conduction properties.

The microstructures of the materials used in the μ-SOFC membrane depend on the chemical composition, the deposition technique used, the post-deposition annealing, and the substrate. It is therefore necessary to find the optimal parameters in order to obtain the desired properties for a high μ-SOFC performance over long-term operation with good stability (e.g. without poisoning or structural degradation).

A large scatter in electrical conductance is found in the ionic conductivity of electrolyte materials with decreasing grain size. Not all the observed behaviors can be explained by existing models, especially as spatial characterization techniques approach their resolution limits. More basic work is needed in order to fully understand the behavior of electrolyte materials with microstructural features in the nanometer range and in order to optimize these components.

The electrodes for μ-SOFC application are also far from optimum—the cathode, in particular, limits the μ-SOFC performance when approaching lower operating temperatures. Coarsening by Ostwald ripening of nanostructured materials is a major concern whenever μ-SOFC membranes are operated at elevated temperatures.

The substrate must be chemically and electrically inert. Foturan® glass-ceramic fulfills these criteria, but wet etching with HF-acid may remain a problem, as it may attack the deposited thin films. Silicon wafers are semi-conducting and therefore require an insulating layer (Si_3N_4 or SiO_2) to avoid electrical short-circuiting; this seems to be more difficult than expected.

Individual components of the microfabricated μ-SOFCs, and especially the electrochemical cell membranes presented in this review, are operating successfully on a laboratory scale today. High performances of 200 mW cm^{-2} can be achieved at rather low operating temperatures—even down to 350 °C! The development of μ-SOFC stacks would provide a sufficient power supply for portable electronic devices. However, a great deal of work is still needed in order to arrive at integrated operating demonstrator systems.

Acknowledgments

Financial support from the below listed Swiss institutions for the ONEBAT and NANCER projects is gratefully acknowledged:

- Commission for Technology and Innovation (CTI);
- Competence Centre for Energy and Mobility (CCEM);
- Competence Centre for Materials Science and Technology (CCMX);
- Bundesamt für Energie (BfE);
- Swiss Electric Research (SER).

References

[1] A. Kundu, J.H. Jang, J.H. Gil, C.R. Jung, H.R. Lee, S.H. Kim, B. Ku, Y.S. Oh, J. Power Sources 170 (2007) 67.
[2] A. Casalegno, P. Grassini, R. Marchesi, Appl. Therm. Eng. 27 (2007) 748.
[3] G.J. La O, H.J. In, E. Crumlin, G. Barbastathis, Y. Shao-Horn, Int. J. Energy Res. 31 (2007) 548.
[4] S.C. Singhal, K. Kendall, High Temperature Solid Oxide Fuel Cells—Fundamentals, Design and Application, Elsevier Advanced Technology, Oxford, 2003.
[5] A. Bieberle-Hutter, D. Beckel, A. Infortuna, U.P. Muecke, J.L.M. Rupp, L.J. Gauckler, S. Rey-Mermet, P. Muralt, N.R. Bieri, N. Hotz, M.J. Stutz, D. Poulikakos, P. Heeb, P. Muller, A. Bernard, R. Gmur, T. Hocker, J. Power Sources 177 (2008) 123.
[6] D. Nikbin, Fuel Cell Rev. (2006) 21.
[7] A.F. Jankowski, J.P. Hayes, R.T. Graff, J.D. Morse, Materials for Energy Storage, Generation and Transport, Materials Research Society, 730 (2002) pp. 93.
[8] S.B. Schaevitz, A. Franz, R. Barton, US 2005/0115889 (2005).
[9] S.B. Schaevitz, A. Franz, R. Barton, A.P. Ludwiszewski, US 2006/0263655 (2006).
[10] A. Infortuna, A.S. Harvey, L.J. Gauckler, Adv. Funct. Mater. 18 (2008) 127.
[11] U.P. Muecke, D. Beckel, A. Bernard, A. Bieberle-Hutter, S. Graf, A. Infortuna, P. Müller, J.L.M. Rupp, J. Schneider, L.J. Gauckler, Adv. Funct. Mater. 18 (2008) 1.
[12] U.P. Muecke, K. Akiba, A. Infortuna, T. Salkus, N.V. Stus, L.J. Gauckler, Solid State Ionics 178 (2008) 1762.
[13] D. Beckel, A. Bieberle-Hutter, A. Harvey, A. Infortuna, U.P. Muecke, M. Prestat, J.L.M. Rupp, L.J. Gauckler, J. Power Sources 173 (2007) 325.
[14] J.L.M. Rupp, A. Infortuna, L.J. Gauckler, J. Am. Ceram. Soc. 90 (2007) 1792.
[15] A. Bieberle-Hutter, D. Beckel, U.P. Muecke, J.L.M. Rupp, A. Infortuna, L.J. Gauckler, MST News 04–05 (2005) 12.
[16] G. Robert, EP 1455409-A1 (2004).
[17] L.J. Gauckler, D. Beckel, U.P. Muecke, P. Müller, J.L.M. Rupp, WO2007/045111 (2007).
[18] L.J. Gauckler, D. Beckel, U.P. Muecke, P. Müller, J.L.M. Rupp, WO2007/045113 (2007).
[19] D. Beckel, L.J. Gauckler, WO2007056876-A1; EP1951641-A1 (2007).
[20] S. Rey-Mermet, P. Muralt, Solid State Ionics 179 (2008) 1497.
[21] S. Rey-Mermet, P. Muralt, J. Baborowski, PCT/EP2006/069688 (2007).
[22] M.J. Stutz, R.N. Grass, S. Loher, W.J. Stark, D. Poulikakos, J. Power Sources 182 (2008) 558.
[23] M.J. Stutz, N. Hotz, D. Poulikakos, Chem. Eng. Sci. 61 (2006) 4027.
[24] M.J. Stutz, W.J. Stark, D. Poulikakos, EP 07012131 (2007).
[25] N. Hotz, M.J. Stutz, S. Loher, W.J. Stark, D. Poulikakos, Appl. Catal. B 73 (2007) 336.
[26] N. Hotz, S.M. Senn, D. Poulikakos, J. Power Sources 158 (2006) 333.
[27] N. Hotz, D. Poulikakos, A.R. Studart, A. Bieberle-Hutter, L.J. Gauckler, EP 08 012273 (2008).
[28] H. Huang, M. Nakamura, P.C. Su, R. Fasching, Y. Saito, F.B. Prinz, J. Electrochem. Soc. 154 (2007) B20.
[29] J.H. Shim, C.C. Chao, H. Huang, F.B. Prinz, Chem. Mater. 19 (2007) 3850.
[30] C.D. Baertsch, K.F. Jensen, J.L. Hertz, H.L. Tuller, S.T. Vengallatore, S.M. Spearing, M.A. Schmidt, J. Mater. Res. 19 (2004) 2604.
[31] P. Jasinski, Microelectron. Int. (2008) 42.
[32] N.M. Sammes, Y. Du, R. Bove, J. Power Sources 145 (2005) 428.
[33] T. Suzuki, Y. Funahashi, T. Yamaguchi, Y. Fujishiro, M. Awano, Electrochem. Solid-State Lett. 10 (2007) A177.

[34] T. Suzuki, Y. Funahashi, T. Yamaguchi, Y. Fujishiro, M. Awano, J. Power Sources (2008) 544.
[35] V.T. Srikar, K.T. Turner, A.T.Y. Ie, S.M. Spearing, J. Power Sources 125 (2004) 62.
[36] J. Fleig, H.L. Tuller, J. Maier, Solid State Ionics 174 (2004) 261.
[37] T.R. Dietrich, W. Ehrfeld, M. Lacher, M. Kramer, B. Speit, Microelectron. Eng. 30 (1996) 497.
[38] Y. Yamazaki, Electrochim. Acta 50 (2004) 663.
[39] H. Huang, P. Su, F.B. Prinz, M. Nakamura, T.P. Holme, R. Fashing, Y. Saito, WO2007084776-A2; US2007184322-A1 (2007).
[40] C.-W. Kwon, J.-W. Son, D.-J. Lee, K.-B. Kim, J.-H. Lee, H.-W. Lee, Fabrication of Thin Film Sofc by Using Aao as Electrode Template, European Fuel Cell Forum, 2008, pp. B0519.
[41] P.C. Su, C.C. Chao, J.H. Shim, R. Fasching, F.B. Prinz, Nano Lett. 8 (2008) 2289.
[42] J.H. Joo, G.M. Choi, J. Power Sources 182 (2008) 589.
[43] S. Rey-Mermet, P. Muralt, Solid State Ionics (2006) 217.
[44] S. Rey-Mermet, Microfabricated Solid Oxide Fuel Cells, PhD thesis (2008).
[45] S. Kang, P.C. Su, Y.I. Park, Y. Saito, F.B. Prinz, J. Electrochem. Soc. 153 (2006) A554.
[46] Y. Tang, K. Stanley, J. Wu, D. Ghosh, J. Zhang, J. Micromech. Microeng. 15 (2005) 185.
[47] R.F. Bunshah, Handbook of Deposition Techniques for Films and Coatings, Noyes Publications, Park Ridge, NJ, 1994.
[48] M. Ohring, The Materials Science of Thin Films: Deposition and Structure, Academic Press, San Diego (CA, USA), London (UK), 2002.
[49] X.H. Wang, H. Huang, T. Holme, X. Tian, F.B. Prinz, J. Power Sources 175 (2008) 75.
[50] J.L.M. Rupp, A. Bieberle-Hütter, A. Evans, H. Galinski, T. Ryll, B. Scherrer, R. Tölke, L.J. Gauckler, Micro-Solid Oxide Fuel Cells: From Thin Films to Power Delivering Membranes, European Fuel Cell Forum, 2008, pp. B0701.
[51] J. Mizusaki, H. Tagawa, T. Saito, K. Kamitani, T. Yamamura, K. Hirano, S. Ehara, T. Takagi, T. Hikita, M. Ippommatsu, S. Nakagawa, K. Hashimoto, J. Electrochem. Soc. 141 (1994) 2129.
[52] A. Bieberle, L.P. Meier, L.J. Gauckler, J. Electrochem. Soc. 148 (2001) A646.
[53] U.P. Muecke, S. Graf, U. Rhyner, L.J. Gauckler, Acta Mater. 56 (2008) 677.
[54] G.J. La O, J. Hertz, H. Tuller, Y. Shao-Horn, J. Electroceram. 13 (2004) 691.
[55] C. Kleinlogel, L.J. Gauckler, Temperature Limitations in the Processing Sequence of Solid Oxide Fuel Cells, Springer, 2000, pp. 359.
[56] M. Godickemeier, L.J. Gauckler, J. Electrochem. Soc. 145 (1998) 414.
[57] C. Kleinlogel, M. Godickemeier, K. Honegger, L.J. Gauckler, Proceedings of the Third International Symposium on Ionic and Mixed Conducting Ceramics, 1998, p. 97.
[58] C. Kleinlogel, L.J. Gauckler, Solid Oxide Fuel Cells (SOFC VI). Proceedings of the Sixth International Symposium, 1999, p. 225.
[59] D. Perednis, K. Honegger, L.J. Gauckler, Fourth European Solid Oxide Fuel Cell Forum Proceedings, 2000, p. 819.
[60] D. Perednis, Solid Oxide Fuel Cells VIII (SOFC VIII) 2003 (2003) 970.
[61] P. Holtappels, T. Graule, B. Gut, U. Vogt, L. Gauckler, M. Jorger, D. Perednis, K. Honegger, G. Robert, S. Rambert, A.J. McEvoy, Solid Oxide Fuel Cells VIII (SOFC VIII) (2003) 1003.
[62] D. Perednis, L.J. Gauckler, Solid State Ionics 166 (2004) 229.
[63] M. Greenberg, E. Wachtel, I. Lubomirsky, J. Fleig, J. Maier, Adv. Funct. Mater. 16 (2006) 48.
[64] D.J. Quinn, B. Wardle, S.M. Spearing, J. Mater. Res. 23 (2008) 609.
[65] J.L.M. Rupp, C. Solenthaler, P. Gasser, U.P. Muecke, L.J. Gauckler, Acta Mater. 55 (2007) 3505.
[66] J.L.M. Rupp, A. Infortuna, L.J. Gauckler, Acta Mater. 54 (2006) 1721.
[67] J.L.M. Rupp, B. Scherrer, A. Harvey, L.J. Gauckler, Adv. Funct. Mater. (2008).
[68] H. Huang, T.M. Gur, Y. Saito, F. Prinz, Appl. Phys. Lett. 89 (2006) 143107.
[69] T. Suzuki, I. Kosacki, H.U. Anderson, Solid State Ionics 151 (2002) 111.
[70] J.L.M. Rupp, L.J. Gauckler, Solid State Ionics 177 (2006) 2513.
[71] A. Bieberle-Hutter, J.L. Hertz, H.L. Tuller, Acta Mater. 56 (2008) 177.
[72] I. Kosacki, T. Suzuki, V. Petrovsky, H.U. Anderson, Solid State Ionics 136 (2000) 1225.
[73] J.H. Joo, G.M. Choi, Solid State Ionics 177 (2006) 1053.
[74] S. Heiroth, T. Lippert, A. Wokaun, M. Döbeli, Appl. Phys. A: Mater. Sci. Process 93 (2008) 639.
[75] I. Kosacki, C.M. Rouleau, P.F. Becher, J. Bentley, D.H. Lowndes, Solid State Ionics 176 (2005) 1319.
[76] J. Garcia-Barriocanal, A. Rivera-Calzada, M. Varela, Z. Sefrioui, E. Iborra, C. Leon, S.J. Pennycook, J. Santamaria, Science 321 (2008) 676.
[77] K.D. Kreuer, Annu. Rev. Mater. Res. 33 (2003) 333.
[78] P. Ranran, W. Yan, Y. Lizhai, M. Zongqiang, Solid State Ionics 177 (2006) 389.
[79] B. Zhu, High-Performance Ceramics III 280–283 (Pts 1 and 2) (2005) 413.
[80] J. Fleig, F.S. Baumann, V. Brichzin, H.R. Kim, J. Jamnik, G. Cristiani, H.U. Habermeier, J. Maier, Fuel Cells 6 (2006) 284.
[81] V. Brichzin, J. Fleig, H.U. Habermeier, G. Cristiani, J. Maier, Solid State Ionics 152 (2002) 499.
[82] A. Bieberle-Hutter, H.L. Tuller, J. Electroceram. 16 (2006) 151.
[83] A. Bieberle-Hutter, M. Sogaard, H.L. Tuller, Solid State Ionics 177 (2006) 1969.
[84] J.L. Hertz, H.L. Tuller, J. Electrochem. Soc. 154 (2007) B413.
[85] C. Peters, A. Weber, E. Ivers-Tiffee, J. Electrochem. Soc. 155 (2008) B730.
[86] B.C.H. Steele, J.M. Bae, Solid State Ionics 106 (1998) 255.
[87] M. Prestat, J.F. Koenig, L.J. Gauckler, J. Electroceram. 18 (2007) 87.
[88] M. Prestat, A. Infortuna, S. Korrodi, S. Rey-Mermet, P. Muralt, L.J. Gauckler, J. Electroceram. 18 (2007) 111.
[89] F.S. Baumann, J. Fleig, G. Cristiani, B. Stuhlhofer, H.U. Habermeier, J. Maier, J. Electrochem. Soc. 154 (2007) B931.
[90] D. Beckel, U.P. Muecke, T. Gyger, G. Florey, A. Infortuna, L.J. Gauckler, Solid State Ionics 178 (2007) 407.
[91] E. Perry Murray, M.J. Sever, S.A. Barnett, Solid State Ionics 148 (2002) 27.
[92] Z.P. Shao, S.M. Haile, Nature 431 (2004) 170.
[93] F.S. Baumann, J. Fleig, H.U. Habermeier, J. Maier, Solid State Ionics 177 (2006) 3187.
[94] F.S. Baumann, J. Maier, J. Fleig, Solid State Ionics (2008) 1198.
[95] M. Heule, L.J. Gauckler, Sens. Actuators B-Chem. 93 (2003) 100.
[96] L.I. Berger, CRC Handbook of Chemistry and Physics, CRC Press/Taylor and Francis, Boca Raton, FL, 2008, pp. 77.